Journal of the Korean Astronomical Society
54: 121 ∼ 128, 2021 August

https://doi.org/10.5303/JKAS.2021.54.4.121
pISSN: 1225-4614 · eISSN: 2288-890X
http://jkas.kas.org

Do the Observed Relations of the Global Seismic Parameters Depend on the Magnetic Activity Level?

Ki-Beom Kim and Heon-Young Chang

Department of Astronomy and Atmospheric Sciences, Kyungpook National University, Daegu 41566, Korea; hyc@knu.ac.kr

Received April 19, 2021; accepted July 1, 2021

Abstract: It has been known that the global asteroseismic parameters as well as the stellar acoustic mode parameters vary with stellar magnetic activity. Some solar-like stars whose variations are thought to be induced by magnetic activity, however, show mode frequencies changing with different magnitude and phase unlike what is expected for the Sun. Therefore, it is of great importance to find out whether expected relations are consistently manifested regardless of the phase of the stellar magnetic cycle, in the sense that observations are apt to cover a part of a complete cycle of stellar magnetic activity unless observations span several decades. Here, we explore whether the observed relations of the global seismic parameters hold good regardless of the phase of the stellar magnetic cycle, even if observations only cover a part of the stellar magnetic cycle. For this purpose, by analyzing photometric Sun-as-a-star data from 1996 to 2019 covering solar cycles 23 and 24, we compare correlations of the global asteroseismic parameters and magnetic proxies for four separate intervals of the solar cycle: solar minima ±2 years, solar minima +4 years, solar maxima ±2 years, and solar maxima +4 years. We have found that the photometric magnetic activity proxy, $S_{\rm ph}$, is an effective proxy for the solar magnetic activity regardless of the phase of the solar cycle. The amplitude of the mode envelope correlates negatively with the solar magnetic activity regardless of the phase of the solar cycle. However, relations between the central frequency of the envelope and the envelope width are vulnerable to the phase of the stellar magnetic cycle.

Key words: asteroseismology — Sun: activity — methods: data analysis

1. Introduction

Helio- and asteroseismology allow us to improve our knowledge of the underlying physics that takes place inside the Sun and solar-like stars through observing non-radial oscillations (Gough 1985, 1990; Aerts et al. 2010; García & Ballot 2019). These are caused by resonant sound waves, stochastically excited by turbulence in near-surface layers of the convective envelope, forming distinct peaks in the acoustic power spectrum (Goldreich & Keeley 1977; Goldreich & Kumar 1988; Balmforth 1992). Helioseismic analysis of the individual frequencies of these peaks thus reveals the solar interior which has been only presumed with a theoretical model constrained by observations of photons from the outermost surface. For example, it has been demonstrated that the solar internal rotation profile is separated into a rigidly-rotating core and a differentially-rotating envelope at the boundary layer known as the tachocline, in which the solar dynamo is thought to work (Fan 2009).

In asteroseismology, thanks to the advent of long and extensive asteroseismic measurements provided by space missions, such as MOST (Walker et al. 2003), CoRoT (Baglin et al. 2006; Michel et al. 2008), *Kepler* (Borucki et al. 2010), and TESS (Ricker et al. 2015), we may infer fundamental stellar parameters such as mass, radius, surface gravity, age, and distance through statistical studies of the asteroseismic scaling relations (Houdek et al. 1999; Samadi et al. 2007; Kjeldsen & Bedding 2011; Belkacem et al. 2011, 2013; Bellinger 2019, 2020; Zinn et al. 2019; Silva Aguirre et al. 2020; Hekker 2020; Kim & Chang 2021a). The asteroseismic scaling relations for the large frequency separation, $\Delta\nu$, and the frequency of the maximum power in the power spectrum, $\nu_{\rm max}$, have in particular caught attention in various fields of astrophysics.

Meanwhile, the stellar magnetic field is considered to play a role in thermal and structural effects on the upper boundary of the acoustic cavity. Owing to the accurate and precise measurement of the solar oscillation frequencies, it has been known for over ∼40 years that solar acoustic mode parameters, including the individual mode frequencies, change with solar activity level (Woodard & Noyes 1985; Fossat et al. 1987; Pallé et al. 1989; Libbrecht & Woodard 1990; Elsworth et al. 1990, 1994; Chaplin et al. 1998, 2001, 2004). Not surprisingly, since the first seismic detection of modulations in the acoustic power spectrum was made in the F5V-star HD49933 using CoRoT satellite data (García et al. 2010), the number of solar-like stars in which activity-related variations are noticed increases rapidly. In inferring fundamental stellar parameters, asteroseismic scaling relations have also provided evidence that the global asteroseismic quantities depend on the stellar magnetic activity. That is, magnetically active stars appear to have a lower envelope amplitude of p-mode

Corresponding author: H.-Y. Chang

power excess than less active stars, when regarding the relation between the envelope amplitude and $\nu_{\rm max}$ (e.g., Huber et al. 2011).

It should be pointed out, however, that some solar-like stars show a different time-lag between temporal variations of mode frequency and amplitude from that found in the solar case (García et al. 2010; Mathur et al. 2013, 2014; Santos et al. 2018). Santos et al. (2018) analyzed 87 solar-like stars measuring temporal frequency shifts and found mode frequencies and amplitudes of ∼20% of the stars changing *in phase*, i.e., opposite to what is found for the Sun. This could be because activity-related variations are encoded in mode parameters with different responsiveness dependent on stellar parameters (Noyes et al. 1984; Chaplin et al. 2007; Metcalfe et al. 2007; Mamajek & Hillenbrand 2008; García et al. 2014; Davies et al. 2015; Broomhall 2017; Karoff et al. 2018), or simply because not all the observed variability is associated with magnetism. Therefore, it is of great importance to critically investigate how the observed variations depend on stellar parameters such as rotational period, age, effective temperature, metallicity. In such an attempt, a homogeneous data sample in stellar parameters is required to carefully single out stellar magnetic cycles (Kim & Chang 2021c).

In this paper, we take another approach in examining whether all the observed variations are consistent with an activity-related origin, in the sense that the unexpected relation between frequency shifts and amplitude changes can be considered as stochastic noise during a particular phase of the stellar magnetic cycle. In other words, we attempt to answer the question whether the observed relations of the global seismic parameters hold good regardless of the phase of the stellar magnetic cycle, even if observations cover only a part of the stellar magnetic cycle. This is an interesting issue since one may insist that activity-induced variations are too subtle to be statistically observed if an observation period falls on a particular phase of the stellar magnetic cycle of a target star by chance. To explore the possibility that the observed relations between parameters of the stellar acoustic oscillations are vulnerable to the phase of the stellar magnetic cycle, we compare relations between the global seismic parameters of the solar acoustic oscillations, which are thought to vary due to an activity-related origin, at various phases of the solar cycle.

We analyze photometric Sun-as-a-star data from January in 1996 to June in 2019 covering solar cycles 23 and 24. We divide the whole time series into 47 segments spanning 6 months each and calculate the global seismic parameters for the stellar oscillation power excess of the corresponding power spectrum. We obtain Pearson's linear correlation coefficient between temporal variations of the global asteroseismic parameters and a proxy for the solar magnetic activity, along with the false alarm probability, as a function of time. Having done that, we compare results from specific periods of the solar cycle such solar minima ±2 years, solar minima +4 years corresponding to a part of the ascending phase, solar maxima ±2 years, and solar maxima +4 years corresponding to a part of the descending phase. We find that the anti-correlated behavior of envelope amplitude and the magnetic activity level seems insensitive to the phase of the magnetic cycle while other relations are not.

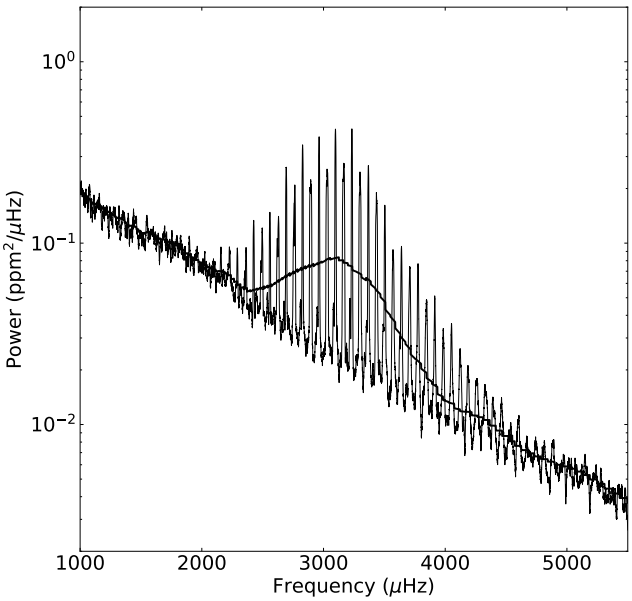

Figure 1. Solar acoustic power spectrum resulting from the time series observed in the second half of 1996, smoothed by a Gaussian moving average with a width of 10 μHz. The thick curve represents the best-fit Gaussian envelope with background-noise components as described in the text.

This paper is organized as follows. We begin with a description of the data analyzed and methods used to acquire p-mode envelope parameters in Section 2. We present the relations between p-mode envelope parameters and solar activity as a whole and in terms of the solar phase in Section 3. Finally, we briefly summarize the results and conclude the study in Section 4.

2. DATA AND METHODS

The Variability of solar Irradiance and Gravity Oscillations (VIRGO) experiment on board the Solar and Heliospheric Observatory (SoHO) aims to investigate the solar deep interior with helioseismic techniques (Fröhlich et al. 1995, 1997). VIRGO includes the three-channel Sun PhotoMeters (SPM) obtaining photometric Sun-as-a-star data continuously since the beginning of 1996, except two unfortunate periods due to temporary malfunctions of the SoHO spacecraft in the summer of 1998 and January 1999. The duty cycle of the time series is around 94%–96%. The VIRGO/SPM observes the Sun as a star at 402 nm (BLUE channel), 500 nm (GREEN channel), and 862 nm (RED channel) over 5-nm passbands. The VIRGO/SPM photometric observations were calibrated as described in Jiménez et al. (2002). The convective background is higher in VIRGO/SPM data than in those from Global Oscillations at Low Frequencies (GOLF), which is another

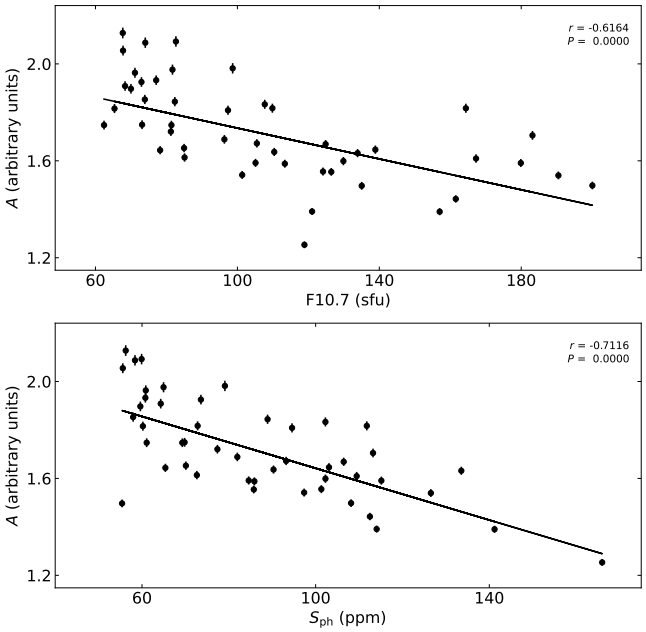

Figure 2. Scatter plots of F10.7 vs. A (top panel), and $S_{\rm ph}$ vs. A (bottom panel) from the entire data set collected from 1996 to 2019. The straight line represents the best linear fit.

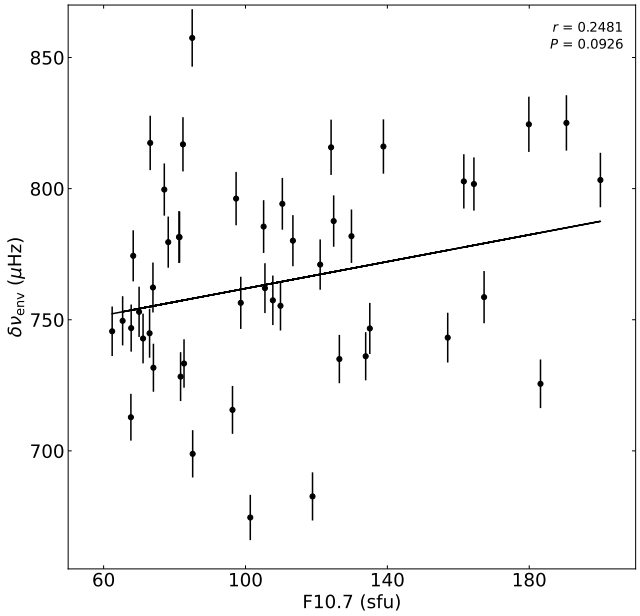

Figure 3. Scatter plot of F10.7 vs. $\delta\nu_{\rm env}$ from the entire data set collected from 1996 to 2019. The straight line represents the best linear fit.

instrument on board SoHO to measure the Doppler velocity of the surface of the Sun (Gabriel et al. 1995, 1997). Thus, the signal-to-noise ratio of the acoustic modes is relatively smaller in photometry (by a factor ∼30) while it reaches a factor of ∼300 in Doppler velocity (García & Ballot 2019).

For the present analysis, we have employed level-2 data[1] recorded every 60 seconds from the GREEN channel of the VIRGO/SPM during the period from 1996 to 2019 covering solar cycles 23 and 24. A number of short gaps, most of which are only a few minutes long, in the time series are filled with zeros, causing background noise in at high frequencies. We removed outliers in the time series which deviate by more than 3σ, and detrended the data with a third-order polynomial function with a 10 days wide filter. By getting rid of slow variations, low-frequency trends due to degradation of the photometers in the color channels are cleaned. To examine characteristics of the solar oscillation power excess as a function of time, we divided the observations into 47 segments of six months length each. We also used three-month long, six-month long, and one-year long time series for comparison and found that a segment length of six months is the most suitable for studying temporal modulations of the solar acoustic oscillations. Finally, we computed a power spectrum from each of the six-month long time series with the Lomb-Scargle algorithm (Lomb 1976; Scargle 1982).

We have also extracted the adjusted 10.7-cm radio flux[2] (F10.7) corrected for variations in the Earth–Sun distance from a database managed by the National Geophysical Data Center. The solar radio flux at a wavelength of 10.7 cm, being measured in solar flux units (sfu; 1 sfu = $10^{-22}\,{\rm W\,m^{-2}\,Hz^{-1}}$), has been measured at the Dominion Radio Astrophysical Observatory in Canada. Since a photometric magnetic activity proxy, $S_{\rm ph}$, is widely used to search for magnetic-field related trends in asteroseismology we adopt and generate $S_{\rm ph}$ (Mathur et al. 2014) for comparison. Here, $S_{\rm ph}$ is defined as the standard deviation of flux measured in a light curve of length five times the rotation period of the star. It is useful particularly when the spectroscopic Mount Wilson S-index is unavailable.

In Figure 1, as an example, we show the solar acoustic power spectrum computed from the time series observed in the second half of 1996, smoothed by a Gaussian moving average with a width of 10 μHz, and the best fit of the Gaussian envelope with background-noise components as defined below, represented by the thin and thick curves, respectively. In the current analysis, to minimize its distortion we adopt the width of 10 μHz rather than a commonly-used broad width for *Kepler* target stars, namely, multiples of the large frequency separation, e.g., $\sim 4\Delta\nu$. According to tests we have carried out in advance of the main analysis, our conclusions are insensitive to the width of the Gaussian function unless the width is broader than $\sim$ 40 μHz. To extract the global seismic parameters with the Levenberg-Marquardt least-squares method, the solar acoustic power spectrum over the frequency range 1000 $\mu{\rm Hz} \le \nu \le 6000$ μHz is used.

The model for the global seismic parameters comprises three parameters: the p-mode power excess due to the solar oscillations, $P(\nu)$, the background white

[1] http://SOHO.nascom.nasa.gov/data/data.html
[2] http://www.ngdc.noaa.gov/stp/solar/solardataservices.html

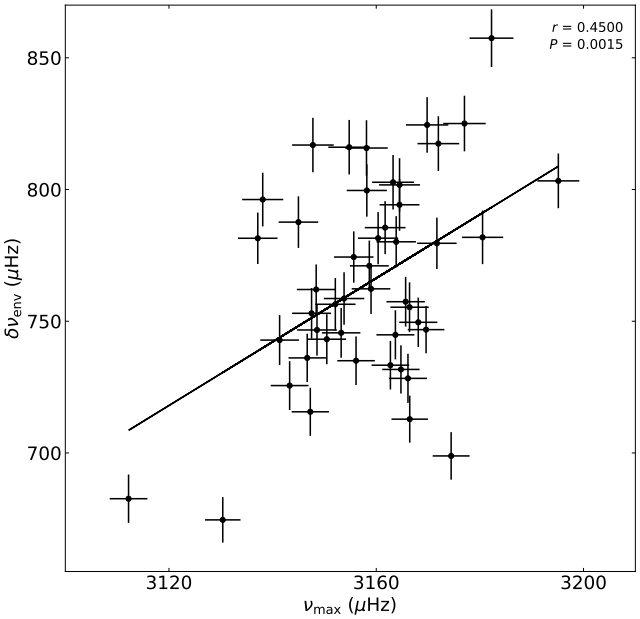

Figure 4. Scatter plot of $\nu_{\rm max}$ and $\delta\nu_{\rm env}$ from the entire data set collected from 1996 to 2019. The straight line represents the best linear fit.

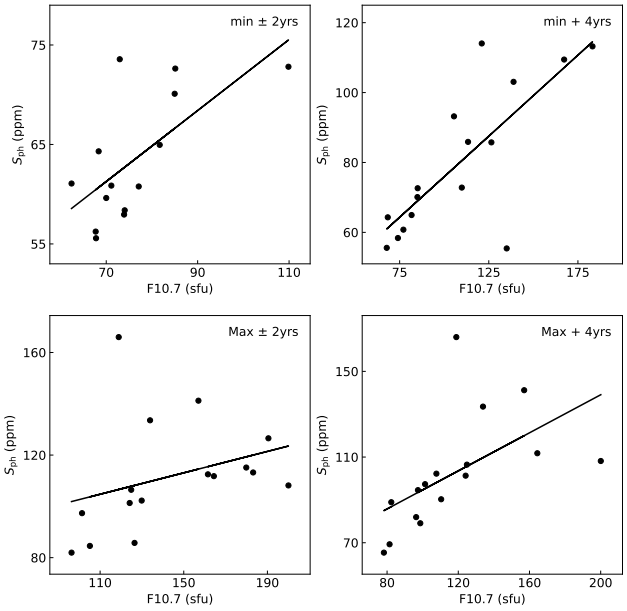

Figure 5. Scatter plots of F10.7 vs. $S_{\rm ph}$ for four separate periods of the solar cycle. The time intervals are indicated in the upper right corner of each panel. The straight lines indicate the best linear fits.

noise caused by photon shots, $W(\nu)$, and the background red noise, $B(\nu)$, due to various phenomena such as granulations on various scales scales, dark spots, bright faculae, and non-periodic fluctuations associated with the chromosphere of the Sun. The oscillation envelope profile, $P(\nu)$, is commonly given by the Gaussian function

$$P(\nu) = A \exp\left[-\frac{(\nu_{\rm max} - \nu)^2}{2\sigma_e^2}\right], \qquad (1)$$

where $\nu_{\rm max}$ is the centroid of the p-mode power excess, A is the amplitude at $\nu_{\rm max}$, and $\delta\nu_{\rm env} = 2\sqrt{2\ln 2}\sigma_e$ is the full width at half maximum. Some F stars, such as Procyon A (Arentoft et al. 2008; Bedding et al. 2010) and HD49933 (Appourchaux et al. 2008), are found to have a broader super-Gaussian shape, causing the parameter values to be biased when the simple Gaussian profile is adopted.

For the background red noise dominating the solar acoustic spectrum at lower frequencies, the acoustic background has been modeled with a number of exponentially decaying functions in the early days of helioseismology (Harvey 1985). The background red-noise is then modeled by relieving the slope as a free parameter as

$$B(\nu) = \sum_i H_i(\nu), \qquad (2)$$

where

$$H_i(\nu) = \frac{4\sigma_g^2\tau_g}{1 + (2\pi\nu\tau_g)^\alpha}, \qquad (3)$$

where σ_g is the rms intensity and τ_g is the characteristic time-scale of the rms intensity (Harvey et al. 1993).

Furthermore, considering that the observed solar acoustic background declines faster as frequency increases, Karoff (2008) has suggested to model the background red noise of the stellar power spectrum like

$$B(\nu) = \sum_{i=1}^{n}\left(\frac{4\sigma_i^2\tau_i}{1 + (2\pi\nu\tau_i)^2 + (2\pi\nu\tau_i)^4}\right), \qquad (4)$$

where σ_i is the i-th component of rms intensity and τ_i is the i-th characteristic time-scale of the rms intensity. Alternatively, one may simply average the power spectrum by binning in equal logarithmic intervals with the median filter (Huber et al. 2009), as we chose to do. By doing so, a reasonable fit can be achieved over a broad frequency range for which physically-motivated empirical models with only a few components can hardly yield a satisfactory fit. For comparison, again, we have repeated the entire analysis with physically-motivated empirical models for the background red noise as well. Nonetheless, in this paper we only provide results by binning in equal logarithmic bins.

3. RESULTS

In Figure 2, we show a scatter plot of F10.7 vs. A and $S_{\rm ph}$ vs. A from the entire data set collected from 1996 to 2019 in the upper and lower panels, respectively. Note that the amplitude is scaled with the background white noise. The straight line shows the the best fit. It is confirmed that the amplitude of the envelope decreases as the solar activity level increases. We calculate the Pearson linear correlation coefficient r together with the probability P that r has an equal or larger value

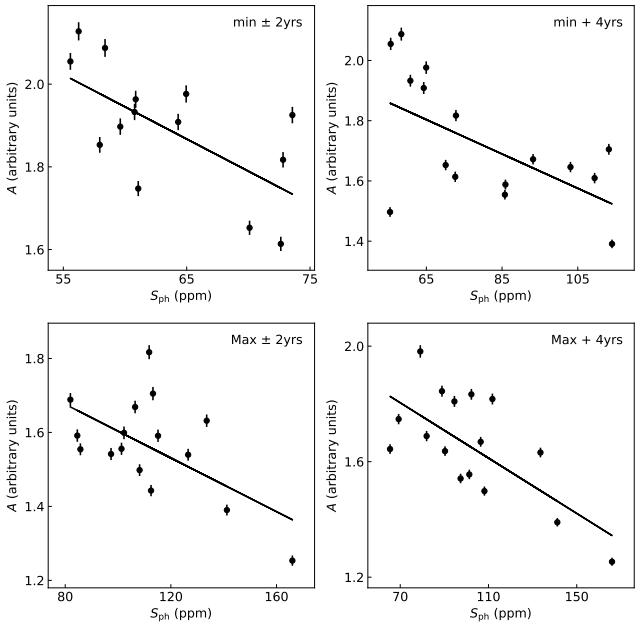

Figure 6. Scatter plots of $S_{\rm ph}$ vs. A for four separate periods of the solar cycle. The time intervals are indicated in the upper right corner of each panel. The straight lines indicate the best linear fits.

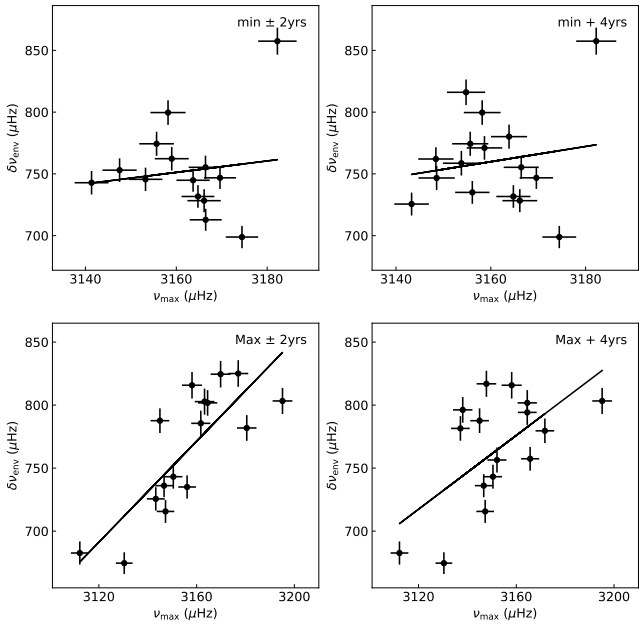

Figure 7. Scatter plots of $\nu_{\rm max}$ vs. $\delta\nu_{\rm env}$ for four separate periods of the solar cycle. The time intervals are indicated in the upper right corner of each panel. The straight lines indicate the best linear fits.

than its observed value by chance. The correlation coefficient between F10.7 and A and the false alarm probability are $r = -0.616$ and $P = 3 \times 10^{-6}$, respectively. For $S_{\rm ph}$ and A, the observed correlation coefficient and chance probability are $r = -0.712$ and $P = 2 \times 10^{-8}$, respectively. The strong anti-correlations between both magnetic proxies and A can be understood by the fact that the individual mode-amplitudes are reduced with increasing solar activity (Chaplin et al. 2003).

In Figure 3, similar to Figure 2, we show a scatter plot of F10.7 vs. $\delta\nu_{\rm env}$ for the entire data set collected from 1996 to 2019. The envelope width of the solar oscillation power excess appears to positively correlate with F10.7 (cf. Karoff 2012). The Pearson linear correlation coefficient and the false alarm probability are $r = 0.248$ and $P = 0.093$, respectively, indicating that F10.7 and $\delta\nu_{\rm env}$ are weakly correlated. A positive correlation between F10.7 and $\delta\nu_{\rm env}$ is explained by a synergy effect of two observational facts. Firstly, since the depression of the individual mode-amplitudes at solar maximum becomes maximal at $\sim \nu_{\rm max}$, whereas reduction rates are negligibly small at both lower and higher frequencies than ~ 3000 μHz, as solar activity continues to its maximum the envelope of the solar oscillations is expected to be more flat than other phases of the solar cycle (Chaplin et al. 2000; Salabert et al. 2003; Kjeldsen et al. 2008; Howe et al. 2015; Kiefer et al. 2018). Secondly, the increase in frequency shift by an activity-related origin is proportional to the mode frequency (Broomhall 2017). Consequently, as solar activity proceeds its cycle to its maximum, the envelope itself is expected to become broader while somehow moving to a high frequency region on average. This is how one may explain the observed statistical behavior of $\delta\nu_{\rm env}$. We would like to point out, however, that the obtained envelope width of the solar p-mode power excess seems to be subject to the signal-to-noise ratio of an individual power spectrum.

In Figure 4, we show a scatter plot of $\nu_{\rm max}$ vs. $\delta\nu_{\rm env}$ for the entire data set. The envelope width of the solar oscillation power excess appears to positively correlate with $\nu_{\rm max}$. The Pearson linear correlation coefficient and the false alarm probability are $r = 0.450$ and $P = 0.002$, respectively, indicating that the two parameters are marginally correlated. Given the positive correlation of the solar acoustic cutoff frequency, $\nu_{\rm ac}$, with solar activity (Jiménez et al. 2011), we may expect a similar correlation of $\nu_{\rm max}$ with solar activity provided that $\nu_{\rm max}$ is proportional to $\nu_{\rm ac}$. Since the observed frequency shifts of the solar p-mode due to solar activity increase with increasing frequency, the envelope itself is also expected not only to become wider but also to move to a higher frequency to some extent (Howe et al. 2020).

In Figure 5, we show scatter plots of F10.7 vs. $S_{\rm ph}$ for four separate periods of the solar cycle: solar minimum ±2 years, solar minimum to solar minimum +4 years (corresponding to a part of the ascending phase), solar maximum ±2 years, and solar maximum to solar maximum +4 years (corresponding to a part of the descending phase), as indicated in the upper right corner of each panel. With these, we are able to see if relations between the global seismic parameters of the solar acoustic oscillations are dependent on a phase of

Table 1
Pearson linear correlation coefficients and false alarm probabilities (in parentheses) for four separate periods.

	min ± 2 years	min + 4 years	Max ± 2 years	Max + 4 years
F10.7 vs. $S_{\rm ph}$	0.6605 (0.0101)	0.7741 (0.0004)	0.3156 (0.2337)	0.5591 (0.0243)
$S_{\rm ph}$ vs. A	−0.6474 (0.0123)	−0.6117 (0.0118)	−0.5722 (0.0205)	−0.6766 (0.0040)
$\delta\nu_{\rm env}$ vs. $\nu_{\rm max}$	0.1838 (0.5294)	0.2080 (0.4395)	0.8006 (0.0002)	0.5987 (0.0143)

the solar magnetic cycle. In Table 1, we list the Pearson linear correlation coefficients of F10.7 vs. $S_{\rm ph}$ for the four separate periods along the corresponding false alarm probabilities (in parentheses).

We find that $S_{\rm ph}$ shows a positive correlation with F10.7 for all cases except the period of solar maxima ±2 years. For that interval, the false alarm probability indicates that the correlation is insignificant. We consider that this is due to large fluctuations in the time series of the years 2003 and 2014, which are both near solar maxima (by selection). From mid-October to early November 2003 one of the most powerful solar storms, called the Halloween solar storm, occurred and photometric light curves are seriously contaminated for an extended period of time. Since $S_{\rm ph}$ is defined as a kind of a the standard deviation, $S_{\rm ph}$ during the period ends up with a much higher value relative to other periods. We could not identify such an energetic event in the 2014 data, but we suspect that the time series has been affected by a similar contamination so that oscillating signals are buried. Reflecting what we have from the current analysis, we conclude that $S_{\rm ph}$ is an effective proxy for the solar magnetic activity regardless of the phase of the solar cycle.

In Figure 6, similar to Figure 5, we show scatter plots of $S_{\rm ph}$ vs. A for four separate periods of the solar cycle together with the best fits. The amplitude of the envelope for the solar oscillation power excess clearly correlates negatively with $S_{\rm ph}$ regardless of the phase of the solar cycle, as shown in Figure 2 for the entire period covering two solar cycles. We list the Pearson linear correlation coefficients together with the false alarm probabilities (in parentheses) in Table 1. All chance probabilities are $\lesssim 2\%$, indicating statistically significant correlations. We conclude that A correlates negatively with the solar magnetic activity regardless of the phase of the solar cycle.

In Figure 7, we show scatter plots of $\delta\nu_{\rm env}$ as a function of $\nu_{\rm max}$ for four separate periods together with the best linear fits. The Pearson linear correlation coefficients are listed, together with the false alarm probabilities (in parentheses), in Table 1. Even though a linear relationship with a positive sign is found by the least-squares fit, the chance probabilities are too high to conclude on the presence of correlations for the intervals of solar minima ±2 years and of solar minima +4 years. Therefore, although one expects a positive correlation between $\nu_{\rm max}$ and $\delta\nu_{\rm env}$ as demonstrated in Figure 4, provided the observation is performed long enough, it turns out that the statistical connection between $\nu_{\rm max}$ and $\delta\nu_{\rm env}$ is the least visible among the global seismic parameters of the solar acoustic oscillations. That is, even though $\nu_{\rm max}$ or $\delta\nu_{\rm env}$ is supposed to correlate with solar activity, we suspect such relations are vulnerable to the phase of the stellar magnetic cycle.

4. SUMMARY AND CONCLUSIONS

It has been known that both acoustic mode parameters and global seismic parameters change with stellar activity level. However, some solar-like stars show mode frequencies and mode amplitudes that vary in phase, in opposition to what is found in the solar power spectrum. This could be because mode parameters respond to the stellar magnetism with different sensitivity or because mechanisms other than magnetic activity contribute to the observed variations during the period around the minimum of the stellar magnetic cycle. Therefore, it is crucial to investigate how the observed variations depend on stellar parameters using carefully prepared homogeneous data.

In this work, we studied whether the observed relationships between parameters of the stellar acoustic oscillations are dependent on the phase of the stellar magnetic cycle. For this purpose, we analyze photometric Sun-as-a-star data covering solar cycles 23 and 24. We divide the entire time series of observations into 47 segments spanning six months each and calculate Pearson's linear correlation coefficient between temporal variations of the global asteroseismic parameters and magnetic proxies as a function of time. We compare results from four separate periods of the solar cycle: solar minima ±2 years, solar minima +4 years (corresponding to a part of the ascending phase), solar maxima ±2 years, and solar maxima +4 years (corresponding to a part of the descending phase).

Our main findings are as follows:

(1) We have confirmed that $S_{\rm ph}$ correlates with F10.7 and found that $S_{\rm ph}$ is an effective proxy for the solar magnetic activity regardless of the phase of the solar cycle.

(2) We have also confirmed that the amplitude of the envelope for the solar oscillation power excess negatively correlates with the solar magnetic activity. Moreover, we conclude that A correlates negatively with the solar magnetic activity regardless of the phase of the solar cycle.

(3) Both $\nu_{\rm max}$ and $\delta\nu_{\rm env}$ correlate with the solar magnetic activity, although the correlations are mostly marginal. However, $\nu_{\rm max}$ correlates positively with $\delta\nu_{\rm env}$, implying that they vary due to an activity-related origin. It should be noted though that such relations are vulnerable to the phase of the stellar magnetic cycle.

It is also an interesting question whether some solar-like stars do not show the expected relations since the stars undergo a particular phase of the stellar magnetic cycle. Based on what we found in our analysis, relations between parameters of the stellar acoustic oscillations hold good regardless of the phase of the stellar magnetic cycle, though for some of those relations the statistical significance is insufficient. Therefore, if the unexpected relations are observed it is because observed variations are due to other mechanisms than a magnetic origin.

Acknowledgments

The VIRGO instrument onboard SoHO is a cooperative effort of scientists, engineers, and technicians, to whom we are indebted. SoHO is a project of international collaboration between ESA and NASA. The authors thank the anonymous referees for critical comments and helpful suggestions. This study was funded by the Basic Science Research Program through the National Research Foundation (NRF) of Korea funded by the Ministry of Science, ICT and Future Planning (grant no. 2018R1A6A1A06024970). HYC was supported by a National Research Foundation of Korea Grant funded by the Korean government (grant no. NRF-2018R1D1A3B070421880).

References

Aerts, C., Christensen-Dalsgaard, J., Kurtz, D. W. 2010, Asteroseismology, Astron. Astrophys. Library (Berlin: Springer)

Appourchaux, T., Michel, E., Auvergne, M., et al. 2008, CoRoT Sounds the Stars: p-mode Parameters of Sun-like Oscillations on HD 49933, A&A, 488, 705

Arentoft, T., Kjeldsen, H., Bedding, T. R., et al. 2008, A Multisite Campaign to Measure Solar-like Oscillations in Procyon. I. Observations, Data Reduction, and Slow Variations, ApJ, 687, 1180

Baglin, A., Auvergne, M., Barge, P., et al. 2006, Scientific Objectives for a Minisat: CoRoT, The CoRoT Mission Pre-Launch Status – Stellar Seismology and Planet Finding, ESA Special Publication, 1306, 33

Balmforth, N. J. 1992, Solar Pulsational Stability – III. Acoustical Excitation by Turbulent Convection, MNRAS, 255, 639

Bedding, T. R., Kjeldsen, H., Campante, T. L., et al. 2010, A Multi-Site Campaign to Measure Solar-Like Oscillations in Procyon. II. Mode Frequencies, ApJ, 713, 935

Belkacem, K., Goupil, M. J., Dupret, M. A., et al. 2011, The Underlying Physical Meaning of the $\nu_{\rm max}$–$\nu_{\rm c}$ Relation, A&A, 530, A142

Belkacem, K., Samadi, R., Mosser, B., et al. 2013, Progress in Physics of the Sun and Stars: A New Era in Helio- and Asteroseismology, ASPC, 479, 61

Bellinger, E. P. 2019, A Seismic Scaling Relation for Stellar Age, MNRAS, 486, 4612

Bellinger, E. P. 2020, A Seismic Scaling Relation for Stellar Age II: The Red Giant Branch, MNRAS, 492, L50

Borucki, W. J., Koch, D., Basri, G., et al. 2010, Kepler Planet-Detection Mission: Introduction and First Results, Science, 327, 977

Broomhall, A.-M. 2017, Seismological Insights into Solar and Stellar Magnetic Activity Cycles, EPJWC, 160, 02009

Chaplin, W. J., Elsworth, Y., Isaak, G. R., et al. 1998, An Analysis of Solar p-mode Frequencies Extracted from BiSON Data: 1991–1996, MNRAS, 300, 1077

Chaplin, W. J., Elsworth, Y., Isaak, G. R., et al. 2000, Variations in the Excitation and Damping of Low-l solar p Modes over the Solar Activity Cycle, MNRAS, 313, 32

Chaplin, W. J., Appourchaux, T., Elsworth, Y., et al. 2001, The Phenomenology of Solar-cycle-induced Acoustic Eigenfrequency Variations: A Comparative and Complementary Analysis of GONG, BiSON and VIRGO/LOI Data, MNRAS, 324, 910

Chaplin, W. J., Elsworth, Y., Isaak, G. R., et al. 2003, Does the Energy Supplied to Low-l Solar p-Modes Vary over the Activity Cycle?, ApJL, 582, L115

Chaplin, W. J., Elsworth, Y., Isaak, G. R., et al. 2004, The Solar Cycle as Seen by Low-l p-mode Frequencies: Comparison with Global and Decomposed Activity Proxies, MNRAS, 352, 1102

Chaplin, W. J., Elsworth, Y., Houdek, G., et al. 2007, On Prospects for Sounding Activity Cycles of Sun-like Stars with Acoustic Modes, MNRAS, 377, 17

Davies, G. R., Chaplin, W. J., Farr, W. M., et al. 2015, Asteroseismic Inference on Rotation, Gyrochronology and Planetary System Dynamics of 16 Cygni, MNRAS, 446, 2959

Elsworth, Y., Howe, R., Isaak, G. R., et al. 1990, Variation of Low-order Acoustic Solar Oscillations over the Solar Cycle, Nature, 345, 322

Elsworth, Y., Howe, R., Isaak, G. R., et al. 1994, Solar p-Mode Frequencies and Their Dependence on Solar Activity: Recent Results from the BISON Network, ApJ, 434, 801

Fan, Y. 2009, Magnetic Fields in the Solar Convection Zone, Living Rev. Sol. Phys., 6, 4

Fossat, E., Gelly, B., Grec, G., et al. 1987, Search for Solar P-Mode Frequency Changes Between 1980 and 1985, A&A, 177, L47

Fröhlich, C., Romero, J., Roth, H., et al. 1995, VIRGO: Experiment for Helioseismology and Solar Irradiance Monitoring, Sol. Phys., 162, 101

Fröhlich, C., Andersen, B. N., Appourchaux, T., et al. 1997, First Results from VIRGO, the Experiment for Helioseismology and Solar Irradiance Monitoring on SOHO, Sol. Phys., 170, 1

Gabriel, A. H., Grec, G., Charra, J., et al. 1995, Global Oscillations at Low Frequency from the SOHO Mission (GOLF), Sol. Phys., 162, 61

Gabriel, A. H., Charra, J., Grec, G., et al. 1997, Performance and Early Results from the GOLF Instrument Flown on the SOHO Mission, Sol. Phys., 175, 207

García, R. A., Mathur, S., Salabert, D., et al. 2010, CoRoT Reveals a Magnetic Activity Cycle in a Sun-Like Star, Science, 329, 1032

García, R. A., Ceillier, T., Salabert, D., et al. 2014, Rotation and Magnetism of Kepler Pulsating Solar-like Stars. Towards Asteroseismically Calibrated Age-rotation Relations, A&A, 572, A34

García, R. A., & Ballot, J. 2019, Asteroseismology of Solar-type Stars, Living Rev. Sol. Phys., 16, 4

Goldreich, P., & Keeley, D. A. 1977, Solar Seismology. II. The Stochastic Excitation of the Solar p-modes by Turbulent Convection, ApJ, 212, 243

Goldreich, P., & Kumar, P. 1988, The Interaction of Acoustic Radiation with Turbulence, ApJ, 326, 462
Gough, D. 1985, Inverting Helioseismic Data, Sol. Phys., 100, 65
Gough, D. O. 1990, Comments on Helioseismic Inference, Progress of Seismology of the Sun and Stars, 367, 283
Harvey, J. 1985, High-Resolution Helioseismology, Future Missions in Solar, Heliospheric & Space Plasma Physics (Noordwijk: ESA), 235, 199
Harvey, J. W., Duvall, T. L., Jefferies, S. M., et al. 1993, Chromospheric Oscillations and the Background Spectrum, ASPC, 42, 111
Hekker, S. 2020, Scaling Relations for Solar-like Oscillations: A Review, Front. Astron. Space Sci., 7, 3
Houdek, G., Balmforth, N. J., Christensen-Dalsgaard, J., et al. 1999, Amplitudes of Stochastically Excited Oscillations in Main-sequence Stars, A&A, 351, 582
Howe, R., Davies, G. R., Chaplin, W. J., et al. 2015, Validation of Solar-cycle Changes in Low-degree Helioseismic Parameters from the Birmingham Solar-Oscillations Network, MNRAS, 454, 4120
Howe, R., Chaplin, W. J., Basu, S., et al. 2020, Solar Cycle Variation of $\nu_{\rm max}$ in Helioseismic Data and its Implications for Asteroseismology, MNRAS, 493, L49
Huber, D., Stello, D., Bedding, T. R., et al. 2009, Automated Extraction of Oscillation Parameters for Kepler Observations of Solar-type Stars, Commun. Asteroseismol., 160, 74
Huber, D., Bedding, T. R., Stello, D., et al. 2011, Testing Scaling Relations for Solar-like Oscillations from the Main Sequence to Red Giants Using Kepler Data, ApJ, 743, 143
Jiménez, A., Roca Cortés, T., & Jiménez-Reyes, S. J. 2002, Variation of the Low-degree Solar Acoustic Mode Parameters over the Solar Cycle, Sol. Phys., 209, 247
Jiménez, A., García, R. A., & Pallé, P. L. 2011, The Acoustic Cutoff Frequency of the Sun and the Solar Magnetic Activity Cycle, ApJ, 743, 99
Karoff, C. 2008, Observational Asteroseismology, Ph.D. Thesis, University of Aarhus
Karoff, C. 2012, Temporal Variations in the Acoustic Signal from Faculae, MNRAS, 421, 3170
Karoff, C., Metcalfe, T. S., Santos, Â. R. G., et al. 2018, The Influence of Metallicity on Stellar Differential Rotation and Magnetic Activity, ApJ, 852, 46
Kiefer, R., Komm, R., Hill, F., et al. 2018, GONG p-Mode Parameters Through Two Solar Cycles, Sol. Phys., 293, 151
Kim, K., & Chang, H. Y. 2021a, Scaling Relations for Width of the Power Excess of Stellar Oscillations, New Astron., 84, 101522
Kim, K., & Chang, H. Y. 2021c, Temporal Variations of the Global Seismic Parameters of HD 49933 over a Magnetic Cycle, JKAS, 54, 129
Kjeldsen, H., Bedding, T. R., Arentoft, T., et al. 2008, The Amplitude of Solar Oscillations Using Stellar Techniques, ApJ, 682, 1370
Kjeldsen, H., & Bedding, T. R. 2011, Amplitudes of Solar-like Oscillations: A New Scaling Relation, A&A, 529, L8
Libbrecht, K. G., & Woodard, M. F. 1990, Solar-cycle Effects on Solar Oscillation Frequencies, Nature, 345, 779
Lomb, N. R. 1976, Least-Squares Frequency Analysis of Unequally Spaced Data, Ap&SS, 39, 447
Mamajek, E. E., & Hillenbrand, L. A. 2008, Improved Age Estimation for Solar-Type Dwarfs Using Activity-Rotation Diagnostics, ApJ, 687, 1264
Mathur, S., García, R. A., Morgenthaler, A., et al. 2013, Constraining Magnetic-activity Modulations in Three Solar-like Stars Observed by CoRoT and NARVAL, A&A, 550, A32
Mathur, S., García, R. A., Ballot, J., et al. 2014, Magnetic Activity of F Stars Observed by Kepler, A&A, 562, A124
Metcalfe, T. S., Dziembowski, W. A., Judge, P. G., et al. 2007, Asteroseismic Signatures of Stellar Magnetic Activity Cycles, MNRAS, 379, L16
Michel, E., Baglin, A., Weiss, W. W., et al. 2008, First Asteroseismic Results from CoRoT, Commun. Asteroseismol. 156, 73
Noyes, R. W., Hartmann, L. W., Baliunas, S. L., et al. 1984, Rotation, Convection, and Magnetic Activity in Lower Main-sequence Stars, ApJ, 279, 763
Pallé, P. L., Regulo, C., & Roca Cortes, T. 1989, Solar Cycle Induced Variations of the Low L Solar Acoustic Spectrum, A&A, 224, 253
Ricker, G. R., Winn, J. N., Vanderspek, R., et al. 2015, Transiting Exoplanet Survey Satellite (TESS), J. Astron. Telesc. Instrum. Syst., 1, 014003-1
Salabert, D., Jiménez-Reyes, S. J., & Tomczyk, S. 2003, Study of p-mode Excitation and Damping Rate Variations from IRIS^{++} Observations, A&A, 408, 729
Samadi, R., Georgobiani, D., Trampedach, R., et al. 2007, Excitation of Solar-like Oscillations across the HR Diagram, A&A, 463, 297
Santos, Â. R. G., Campante, T. L., Chaplin, W. J., et al. 2018, Signatures of Magnetic Activity in the Seismic Data of Solar-type Stars Observed by Kepler, ApJS, 237, 17
Scargle, J. D. 1982, Studies in Astronomical Time Series Analysis. II. Statistical Aspects of Spectral Analysis of Unevenly Spaced Data, ApJ, 263, 835
Silva Aguirre, V., Stello, D., Stokholm, A., et al. 2020, Detection and Characterization of Oscillating Red Giants: First Results from the TESS Satellite, ApJL, 889, L34
Walker, G., Matthews, J., Kuschnig, R., et al. 2003, The MOST Asteroseismology Mission: Ultraprecise Photometry from Space, PASP, 115, 1023
Woodard, M. F., & Noyes, R. W. 1985, Change of Solar Oscillation Eigenfrequencies with the Solar Cycle, Nature, 318, 449
Zinn, J. C., Pinsonneault, M. H., Huber, D., et al. 2019, Testing the Radius Scaling Relation with Gaia DR2 in the Kepler Field, ApJ, 885, 166